Evaluating the Accuracy of a High-Resolution Model Simulation through Comparison with MODIS Observations

YONG-KEUN LEE, JASON A. OTKIN, AND THOMAS J. GREENWALD

Cooperative Institute for Meteorological Satellite Studies, University of Wisconsin—Madison, Madison, Wisconsin

(Manuscript received 22 April 2013, in final form 22 November 2013)

ABSTRACT

Synthetic infrared brightness temperatures (BTs) derived from a high-resolution Weather Research and Forecasting (WRF) model simulation over the contiguous United States are compared with Moderate Resolution Imaging Spectroradiometer (MODIS) observations to assess the accuracy of the model-simulated cloud field. A sophisticated forward radiative transfer model (RTM) is used to compute the synthetic MODIS observations. A detailed comparison of synthetic and real MODIS 11-μm BTs revealed that the model simulation realistically depicts the spatial characteristics of the observed cloud features. Brightness temperature differences (BTDs) computed for 8.5–11 and 11–12 μm indicate that the combined numerical model–RTM system realistically treats the radiative properties associated with optically thin cirrus clouds. For instance, much larger 11–12-μm BTDs occurred within thin clouds surrounding optically thicker, mesoscale cloud features. Although the simulated and observed BTD probability distributions for optically thin cirrus clouds had a similar range of positive values, the synthetic 11-μm BTs were much colder than observed. Previous studies have shown that MODIS cloud optical thickness values tend to be too large for thin cirrus clouds, which contributed to the apparent cold BT bias in the simulated thin cirrus clouds. Errors are substantially reduced after accounting for the observed optical thickness bias, which indicates that the thin cirrus clouds are realistically depicted during the model simulation.

1. Introduction

Numerical weather prediction (NWP) models are an indispensable tool for weather forecasting and long-term climate predictions. To better characterize the accuracy of cloud microphysical parameterization schemes used by high-resolution NWP models, detailed evaluations of the model-simulated cloud fields are necessary. Conventional observing systems, such as radiosondes, provide valuable information about moisture and thermodynamic variables, but do not contain sufficient resolution to effectively evaluate the accuracy of high-resolution NWP model simulations. Satellite measurements, however, contain much higher spatial resolution with global coverage that permits a more comprehensive evaluation of the simulated cloud fields. Many prior studies have utilized satellite observations to evaluate the performance of NWP simulations (e.g., Chaboureau and Pinty 2006; Greenwald et al. 2010; Han et al. 2013; Jankov et al. 2010; Keil et al. 2003; Lopez et al. 2003; Morcrette 1991; Nam and Quaas 2012; Otkin and Greenwald 2008; Otkin et al. 2009; Ringer et al. 2003; Satoh et al. 2010; Sun and Rikus 2004; Tselioudis and Jakob 2002; Yu et al. 1996; Zhang et al. 2001).

Substantial increases in computing resources during the past few years have permitted the temporal and spatial resolution of NWP model simulations to become more comparable to those of satellite measurements. Because of these improvements, a major effort within the Geostationary Operational Environmental Satellite-R Series (GOES-R) program has been to generate synthetic or ''proxy'' top-of-the-atmosphere radiance datasets for the Advanced Baseline Imager (ABI; Schmit et al. 2005) using vertical profiles of temperature, water vapor, and clouds from high-resolution Weather Research and Forecasting (WRF) model simulations. Synthetic satellite datasets are an attractive option for satellite algorithm development and demonstration activities since they can be configured to represent the

Denotes Open Access content.

Corresponding author address: Yong-Keun Lee, CIMSS, University of Wisconsin—Madison, 1225 West Dayton St., Madison, WI 53706.
E-mail: yklee@ssec.wisc.edu

DOI: 10.1175/JAMC-D-13-0140.1

spectral, spatial, and temporal characteristics of the satellite sensor. Such datasets are most useful for these activities if they contain realistic cloud characteristics (Otkin et al. 2007b), which is contingent upon the numerical model accurately simulating the evolution of the atmosphere and cloud morphology. Bikos et al. (2012) discuss the advantages of using synthetic GOES-R ABI brightness temperature (BT) datasets derived from National Severe Storms Laboratory 4-km-resolution WRF model simulations run daily over the conterminous United States (CONUS) to demonstrate ABI measurement capabilities and to prepare researchers and forecasters to utilize the wealth of information that it will provide.

Since Morcrette (1991) first compared synthetic satellite imagery from NWP models with observed satellite BTs using a ''model-to-satellite approach,'' many studies have utilized satellite BTs to evaluate model performance (Chaboureau and Pinty 2006; Han et al. 2013; Jankov et al. 2010; Keil et al. 2003; Otkin and Greenwald 2008; Otkin et al. 2009; Ringer et al. 2003; Sun and Rikus 2004). These studies have demonstrated the advantage of using satellite data and a model-to-satellite approach to validate numerical model results. The satellite BT imagery is useful for weather forecasting because it provides an integrated perspective of the surface, cloud, water vapor, and radiation, from the top of the atmosphere. As NWP and radiative transfer models (RTMs) become more sophisticated, comprehensive comparisons of observed and synthetic satellite BTs will continue to provide very relevant information that can be used to identify model errors and to improve microphysical schemes.

Several recent studies have investigated the accuracy of model-derived proxy datasets having similar spatial and temporal resolutions to satellite observations. Otkin et al. (2009) demonstrated that synthetic Spinning Enhanced Visible and Infrared Imager (SEVIRI) infrared BT computed using output from a large-scale WRF model simulation with 3-km horizontal resolution contained a realistic cloud field with reasonable errors. Using observations from the Cloud Profiler Radar on board the *CloudSat* polar-orbiting satellite, Greenwald et al. (2010) showed that the vertical structure of the simulated cloud field was similar to that observed in several *CloudSat* cloud regimes, including cirrus and low-level cloud, thick cirrus, midlevel convection, and frontal precipitation.

In this study, the accuracy of the simulated cloud field, including thin cirrus clouds, contained in a CONUS-scale simulation with 2-km horizontal resolution is evaluated through a comparison of synthetic and observed BTs from the Moderate Resolution Imaging Spectroradiometer (MODIS). MODIS products provide operational comprehensive information about atmospheric status, including visible and infrared band radiances, as well as cloud physical and optical properties (Platnick et al. 2003). Since thin cirrus clouds modulate solar and longwave radiation through scattering and absorption and therefore strongly affect the Earth–atmosphere system (Chen et al. 2000; Lee et al. 2010), they have been one of the many interesting topics in the atmospheric sciences. Prior studies have used satellite observations to examine cirrus cloud extent in numerical simulations (Garand and Nadon 1998; Gehlot and Quaas 2012); however, no study has directly compared differences in BTs between simulated and observed thin cirrus clouds.

Details about the data and methodology are given in section 2. Simulated and observed MODIS BTs are compared in section 3, with a summary given in section 4.

2. Datasets and method

a. *WRF simulation*

Version 2.2 of the WRF model (Skamarock et al. 2005) was used for this study. WRF is a sophisticated nonhydrostatic NWP model that includes prognostic equations for the horizontal and vertical wind components, various cloud microphysical quantities, and the perturbation geopotential, potential temperature, and surface pressure of dry air. The simulation was performed at the National Center for Supercomputing Applications at the University of Illinois at Urbana–Champaign. It was initialized at 0000 UTC 4 June 2005 using 1° Global Data Assimilation System analyses and then run for 30 h using a triple-nested domain configuration. The massive simulation required 1 TB of physical memory and ~74 000 CPU hours to complete. The outermost domain covered most of the GOES-R full-disk viewing area with 6-km horizontal resolution while the inner domains covered a smaller CONUS and mesoscale regions with 2- and 0.667-km horizontal resolutions, respectively, and 52 vertical levels. This domain configuration was chosen to mimic a potential ABI scanning strategy that may be employed after GOES-R is launched. Subgrid-scale processes were parameterized using the Thompson et al. (2008) microphysics scheme, the Eta Model planetary boundary layer (Mellor and Yamada 1982), and the Dudhia (1989) shortwave and Rapid Radiative Transfer Model (Mlawer et al. 1997) longwave radiation schemes. The Noah land surface model was used to compute surface heat and moisture fluxes. No cumulus parameterization scheme was used. This study solely focuses on evaluating results from the CONUS domain from 1500 to 2130 UTC on 4 June 2005. This domain was used for this study because of its relatively high spatial resolution (2 km) and large geographical extent. Simulated data are available every 15 min during this time period. It

should be noted that the WRF model version used in this study was released six years ago and, thus, the parameterization schemes have undergone further development since then. However, because this simulation has been provided to numerous GOES-R program scientists for satellite algorithm development and demonstration activities (Daniels et al. 2012; Li et al. 2012; Otkin et al. 2007a; Schmit et al. 2012), its evaluation is still useful and the age of the model version does not reduce the validity of the study.

b. *Forward Radiative Transfer Model*

The University of Wisconsin/Space Science and Engineering Center (UW/SSEC) Fast Solar/IR Radiative Transfer Model (Greenwald et al. 2008) is used during this study to produce simulated MODIS infrared BTs. It is based on the successive-order-of-interaction methodology (Heidinger et al. 2006), with inputs such as model-simulated temperature, water vapor, clouds, surface emissivity, and climatological ozone. Several steps are included in the RTM calculations. The Compact-OPTRAN algorithm, available in the Community Radiative Transfer Model (CRTM; Chen et al. 2012; McMillin et al. 2006), is used to compute gas optical depths for each model layer from WRF-simulated outputs. Ice absorption and scattering properties, such as extinction efficiency, single-scattering albedo, and asymmetry factor, are calculated based on Baum et al. (2005) for each frozen hydrometeor species (e.g., ice, snow, and graupel) simulated by the Thompson microphysics scheme. A lookup table based on Lorenz–Mie calculations is used to get absorption and scattering properties for liquid-phase hydrometeors (cloud water and rainwater). Visible cloud optical thickness (COT) is calculated separately for frozen and liquid water phase following Heymsfield et al. (2003) and Han et al. (1995), respectively. Visible COT is converted into infrared COT through a scaling by extinction efficiency. Infrared COT is divided by the cosine of the viewing zenith angle (>0) to consider changes in absorption and scattering due to pathlength. Surface emissivity is obtained from the Seemann et al. (2008) dataset for land surfaces and from CRTM Infrared Sea Surface Emissivity Model for water surfaces.

c. *MODIS data*

MODIS is one of the key instruments on the polar-orbiting *Terra* and *Aqua* satellites. MODIS measures radiances in 36 spectral bands from visible to infrared with horizontal resolutions of 250 m or 500 m for visible and near-infrared bands and 1000 m for infrared bands. MODIS products provide several cloud parameters, including cloud-top pressure (CTP), visible COT, and cloud phase. MODIS collection 5 data from *Aqua* and *Terra* orbital tracks over the CONUS model domain during the simulation period are used for this study. *Aqua* passes over CONUS four times during daytime near 1645, 1815, 1955, and 2130 UTC in ascending mode and *Terra* passes over CONUS also four times during daytime near 1500, 1645, 1815, and 2000 UTC in descending mode on 4 June 2005. Note that MODIS COT is available only during the daytime because visible reflectances are required for its computation. Three MODIS bands are selected for the comparison of BTs between the observations and the simulation, including band 29 (8.5 μm), band 31 (11 μm), and band 32 (12 μm).

To be consistent with the MODIS CTP product, the CO_2 slicing method (Menzel et al. 1983, 2010; Wylie and Menzel 1999) is used to retrieve the CTP from the synthetic MODIS BT in spectral bands within the broad 15-μm CO_2 absorption region. Since the atmosphere becomes more opaque owing to CO_2 absorption as the wavelength increases from 13.3 to 15 μm, the radiances measured from these CO_2 absorption bands are sensitive to different layers in the atmosphere. MODIS bands 31 and 33–36 near 15 μm are used for the CO_2 slicing method. The simulated COT is obtained through the relationship between observed COT and ice water path based on Heymsfield et al. (2003), while the MODIS COT is derived from reflectance lookup tables at shortwave channels including 0.645, 0.858, 1.24, and 2.13 μm.

In this study, thin cirrus cloud from both MODIS observations and the simulation is defined when the CTP is less than 440 hPa, and COT is less than 5. Thin cirrus cloud cases are searched over the whole CONUS model domain for the simulation and the observations. While selecting thin cirrus cloud cases, some optically thin cloud pixels along cloud edges may be neglected in the MODIS dataset because COT retrievals are only performed in regions of homogeneous cloud cover (http://modis-atmos.gsfc.nasa.gov/C005_Changes/C005_CloudOpticalProperties_ver311.pdf). Since this study focuses on a general overview of the WRF simulation over the full model domain (refer to section 3), this issue has minimal impact on the results. WRF outputs are selected at 1645, 1815, 2000, and 2130 UTC, corresponding to the *Aqua* overpasses, and at 1500, 1645, 1815, and 2000 UTC, corresponding to the *Terra* overpasses, for the BT comparison on 4 June 2005.

3. Results

a. *Case study description*

This section provides a comparison of the simulated and observed large-scale atmospheric conditions that

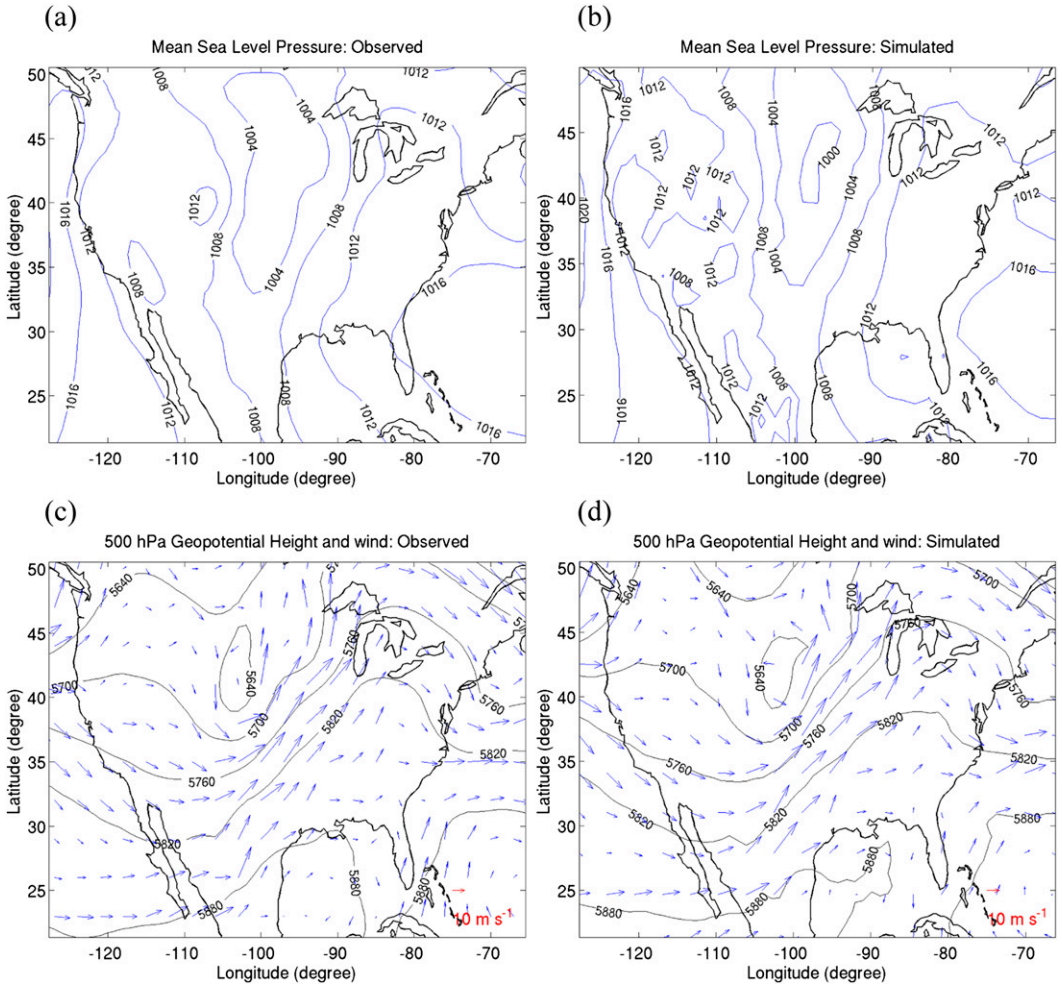

FIG. 1. Mean sea level pressure (hPa) from (a) GDAS and (b) WRF simulations, and 500-hPa geopotential height and wind vectors from (c) GDAS and (d) WRF simulations at 1800 UTC 4 Jun 2005.

occurred during the case study. Figure 1 shows the mean sea level pressure and 500-hPa geopotential heights and winds at 1800 UTC on 4 June 2005 over the CONUS. At this time, a surface low pressure system was located near a strong upper-level jet that extended across the central United States from northern Texas to the upper Midwest. Along and to the east of these features, lifted index values were less than −6°C, with convective available potential energy (CAPE) values larger than 2500 J kg^{-1} both in the observations and the simulation (not shown), which indicates that substantial instability was present within this region. The lifted index is a measure of atmospheric stability, with negative (positive) values indicative of unstable (stable) atmospheric conditions. The lifted index less than −6 denotes very unstable atmospheric conditions. CAPE is also an atmospheric stability index. When CAPE is larger than 2500 J kg^{-1}, the atmosphere is considered to be very unstable. According to the Storm Prediction Center's storm database, there were over 30 tornado reports in this region. High sea level pressure areas are located both in the Pacific Ocean and the Atlantic Ocean and another elongated low pressure area following the east coast of the United States. Overall, the WRF simulation realistically depicts the location and intensity of the surface cyclone and the slight westward tilt of the corresponding upper-level disturbance. Areas of higher surface pressure along the Pacific coast and over the eastern United States are also well simulated.

b. *Brightness temperature comparison*

Figure 2 shows composite images of the observed and simulated MODIS band 31 (11 μm) BTs computed for four consecutive *Aqua* overpasses at 1645, 1815, 1955, and 2130 UTC 4 June 2005. Simulated and observed CTP and COT composites are also shown for the same

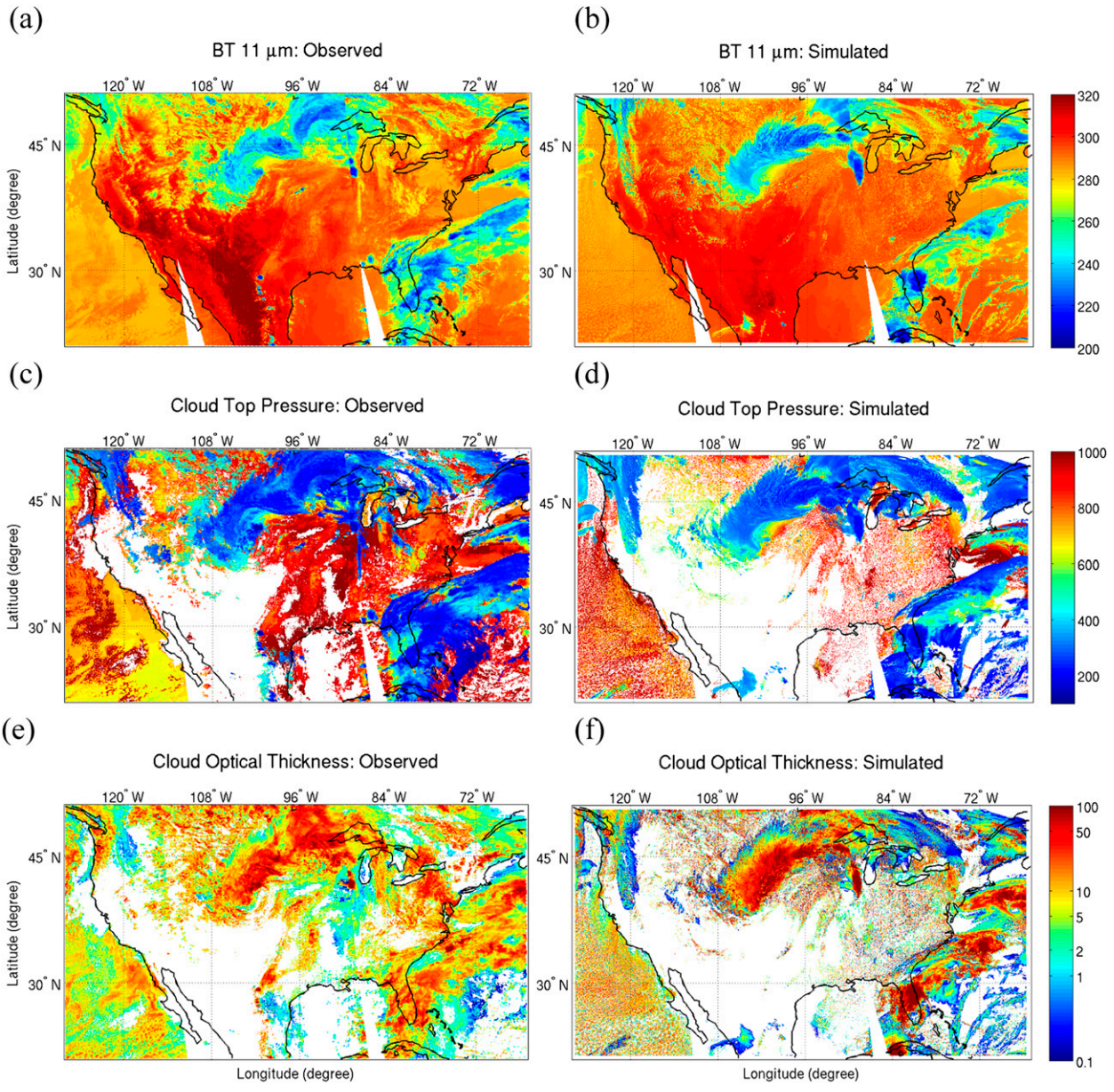

FIG. 2. Composite images of (left) observed and (right) simulated (a),(b) MODIS 11-μm BT (K), (c),(d) CTP (hPa), and (e),(f) visible COT. Four daytime *Aqua* MODIS overpasses at 1645, 1815, 1955, and 2130 UTC 4 Jun 2005 and corresponding WRF-simulated fields at 1645, 1815, 2000, and 2130 UTC are included in the composites.

time period. MODIS band 31 is a window channel used to detect surface and cloud features. Although some discrepancies are apparent in the simulated BT, CTP, and COT composites, several areas of high-, mid-, and low-level cloud cover are realistically depicted in the WRF simulation. For instance, separate regions of upper-level clouds and deep convection over the north-central United States and near Florida exhibiting colder BTs (or thicker COT) closely correspond to the surface low pressure and upper-level trough region where appropriate conditions are present for deep cloud formation. Warmer BTs occur within clear-sky areas and for regions with low-level cloudiness and optically thin upper-level clouds. Since *Aqua* (ascending) and *Terra* (descending) orbits are within 3-h time difference, composite images of the observed and simulated *Terra* MODIS 11-μm BTs contain similar cloud features (not shown). More clear areas in *Terra* MODIS swaths are present, however, over the Gulf of Mexico, southern United States, and northeastern and northwestern areas in the model domain.

The simulated and observed probability distributions for MODIS 11-μm BTs are shown in Fig. 3, computed using all grid points located within each of the *Aqua* and *Terra* MODIS overpass swaths during the simulation period. The simulated distribution is broadly consistent with the observations for both *Aqua* and *Terra*; however, some notable differences are present. In Figs. 3a and 3b, the primary peak near 280 K is slightly warmer and weaker in the simulated dataset primarily because of more lower-level simulated cloudiness over the Pacific Ocean (Figs. 2a–d). The reduced midlevel cloud cover within the northwestern portion and the eastern United States of the domain leads to warmer BTs, thereby contributing to the development of a secondary peak near 295 K in the simulated dataset over *Aqua* and *Terra* orbits in Fig. 3. Meanwhile, over *Terra* overpass swaths, MODIS observes more clear areas than *Aqua* (not shown), and thus the observations also show a secondary peak near 295 K in Fig. 3b. A lower occurrence of simulated BTs $>$ 310 K for both Figs. 3a and 3b may be due to the WRF land surface model underestimating surface temperatures within the sparse vegetation areas of Mexico and the southwestern United States (Fig. 2b). Since the 11-μm channel is used to look at the surface under clear-sky conditions, the lower occurrence of simulated 11-μm BTs $>$ 310 K relative to the observations indicates that the WRF simulation did not fully represent land surface processes in those areas. The distributions are similarly decreasing for 11-μm BTs $<$ 250 K in Figs. 3a and 3b, indicating that the simulated and observed cloud fields have a similar proportion of upper-level clouds. The correlation coefficients between the observed and simulated 11-μm BT probability distributions are 0.81 and 0.83 for *Aqua* and *Terra*, respectively (Table 1). The probability distributions for MODIS bands 29 (8.5 μm) and 32 (12 μm) are similar to that of MODIS band 31 for each overpass (not shown).

The CTP probability distributions of MODIS observations in Figs. 3c and 3d contain three peaks located from 200 to 400, from 600 to 800, and from 800 to 1000 hPa for both the *Aqua* and *Terra* swaths. The WRF simulation represents these three peaks well; however, the probability distribution values of the simulations are larger between 200 and 400 hPa and smaller at lower levels than those of the observations. This is because the WRF simulation defines much of the observed lower-level cloud area as is clearly shown in Figs. 2c and 2d, and therefore, the percentage of the higher-level clouds becomes relatively larger than that of the lower-level clouds in the simulation. In Table 1, correlation coefficients of BT at three bands are over 0.8 for all-sky conditions. The correlation coefficients of COT are noticeably lower than for other parameters in Table 1. Since cirrus detection based on the MODIS measurements has a lower threshold of approximate 0.2–0.3 (Dessler and Yang 2003; Lee et al. 2006), the probability distribution value of MODIS COT $<$ 1 is very low compared to that of the simulation, and it causes lower correlation coefficients between the observed and simulated COT values for both *Aqua* and *Terra*.

c. *Brightness temperature difference comparison*

In this section, the accuracy of the synthetic BT dataset will be assessed through a comparison of 8.5–11- and 11–12-μm brightness temperature difference (BTD) combinations. The BTD technique is used to detect clouds and to infer cloud-top properties based on different radiative properties of cloud particles within each band (Ackerman et al. 1990; Baum et al. 2000a; Strabala et al. 1994). Since ice and water particles have distinct absorption features within these three channels (Strabala et al. 1994; Baum et al. 2000a), the presence of realistic BTDs in the simulated dataset will provide additional evidence that the simulated cloud properties are realistic.

Figure 4 shows composite observed and simulated 8.5–11- and 11–12-μm BTDs for *Aqua* overpasses over the CONUS domain. The distribution of the BTDs for the *Terra* overpasses is similar to those of *Aqua* (not shown). A qualitative comparison of the images shows that the simulated BTDs realistically represent the observed features. Menzel et al. (2010) and Baum et al. (2000a) showed that 8.5–11-μm BTDs are typically positive for ice clouds and negative for water clouds due to the different absorption features of ice and liquid cloud particles at 8.5 and 11 μm. Clear-sky 8.5–11-μm BTDs tend to be negative because the surface emissivity at 8.5 μm tends to be lower than that at 11 μm and the atmospheric water vapor absorption is stronger at 8.5 μm than at 11 μm (Strabala et al. 1994). The correlation coefficients between the observed and simulated 8–11-μm BTD probability distributions are 0.78 and 0.67 for *Aqua* and *Terra*, respectively (Table 1). Greater atmospheric water vapor absorption and ice and water particle absorption at 12 μm than at 11 μm causes the 11–12-μm BTDs to be positive in most regions (Strabala et al. 1994). The emissivity of clouds also affects the 11–12-μm BTDs. Emissivity values increase as COT increases (Platt and Harshvardhan 1988), which reduces the effect of the atmosphere below cirrus cloud layers, and therefore the 11–12-μm BTD decreases as COT increases for cirrus clouds. For example, 11–12-μm BTD values in thin cirrus cloud areas are positive, distinguishing them from thick cirrus cloud areas where BTD values are nearly zero (Figs. 4c,d). The correlation coefficients between the observed and simulated 11–12-μm BTD probability distributions for all-sky conditions are

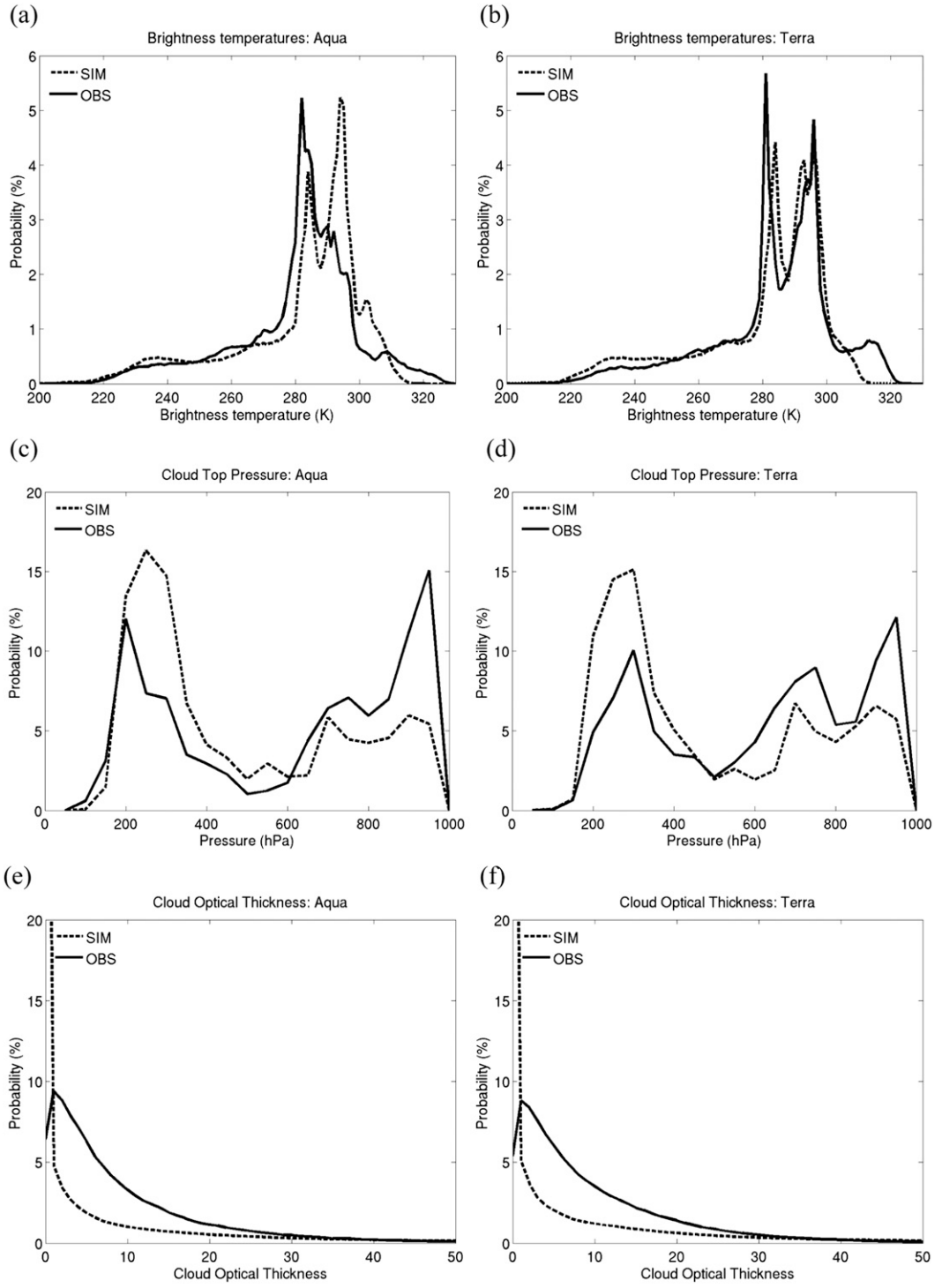

FIG. 3. Simulated (dashed) and observed (solid) probability (%) distributions computed using all grid points in the MODIS swaths over the CONUS region on 4 Jun 2005. Shown are (top) 11-μm BT, (middle) cloud-top pressure, and (bottom) cloud optical thickness for (left) *Aqua* and (right) *Terra*.

TABLE 1. For *Aqua* and *Terra*, correlation coefficients between observed and simulated BT–BTD for different wavelengths and bands; and for the COT and CTP probability distributions for all-sky conditions.

	8.5 μm	11 μm	12 μm	8.5–11 μm	11–12 μm	COT	CTP
Aqua	0.83	0.81	0.83	0.78	0.78	0.38	0.58
Terra	0.86	0.83	0.84	0.67	0.79	0.36	0.63

0.78 and 0.79 for *Aqua* and *Terra*, respectively (Table 1), which are not much degraded compared to those of the 11- and 12-μm BT probability distributions. These correlation coefficients indicate that the combined NWP and RTM system realistically treats the radiative properties of clouds and water vapor.

In Figs. 4a and 4b, deep convective clouds and high-level clouds within the extratropical cyclone over the north-central United States and along the southeastern U.S. coast show large positive values of 8.5–11-μm BTD, whereas lower-level clouds over the eastern United States and in the eastern Pacific Ocean show slightly negative BTD values. Clear-sky regions over the western United States show large negative 8.5–11-μm BTD values since the surface emissivity at 8.5 μm is much lower than at 11 μm over this region.

In Figs. 4c and 4d, as mentioned above, due to the absorption features at 11 μm and 12 μm, 11–12-μm BTDs tend to be positive in most regions. Near-zero BTD values are present in both the observed and model-simulated BTs within the optically thick clouds over the central United States and western Atlantic Ocean; whereas larger positive BTD values (>2 K) occur within the optically thin cirrus clouds surrounding these areas of optically thicker cloud cover. The areas of thin cirrus clouds correspond to regions of warmer 11-μm BTs (Fig. 2). Some clear areas over the eastern part of United States also have larger 11–12-μm BTD values due to more abundant low-level moisture than is found in the surrounding areas (not shown). Since the simulation has larger values of 11–12-μm BTD than those of MODIS, the simulated moisture amount in this area may be larger than actually occurred. Along the western coast of the United States, slightly negative values of the MODIS 11–12-μm BTD are not well depicted in the simulation.

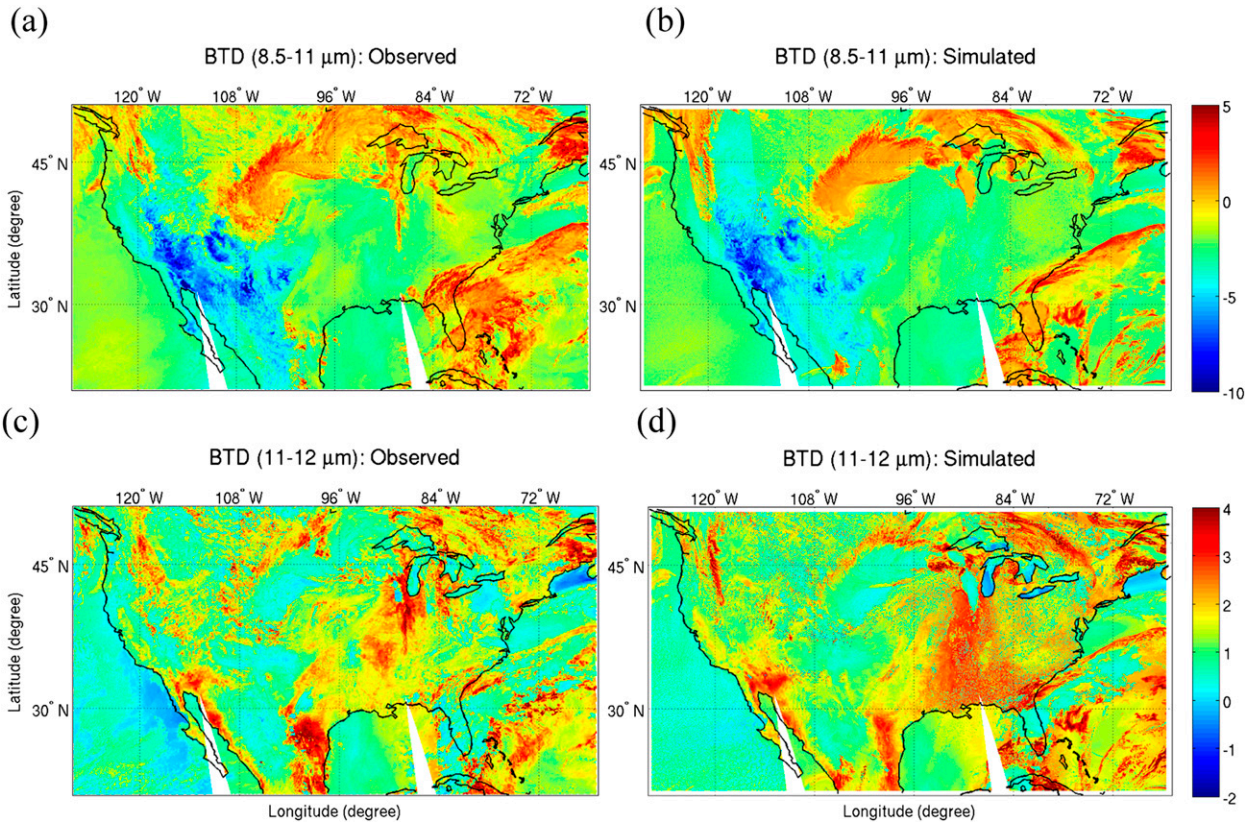

FIG. 4. Composite BTD images constructed using observations from four *Aqua* MODIS overpasses (1645, 1815, 1955, and 2130 UTC) on 4 Jun 2005 and the corresponding simulations. (a) Observed and (b) simulated 8.5–11-μm BTDs, and (c) observed and (d) simulated 11–12-μm BTDs.

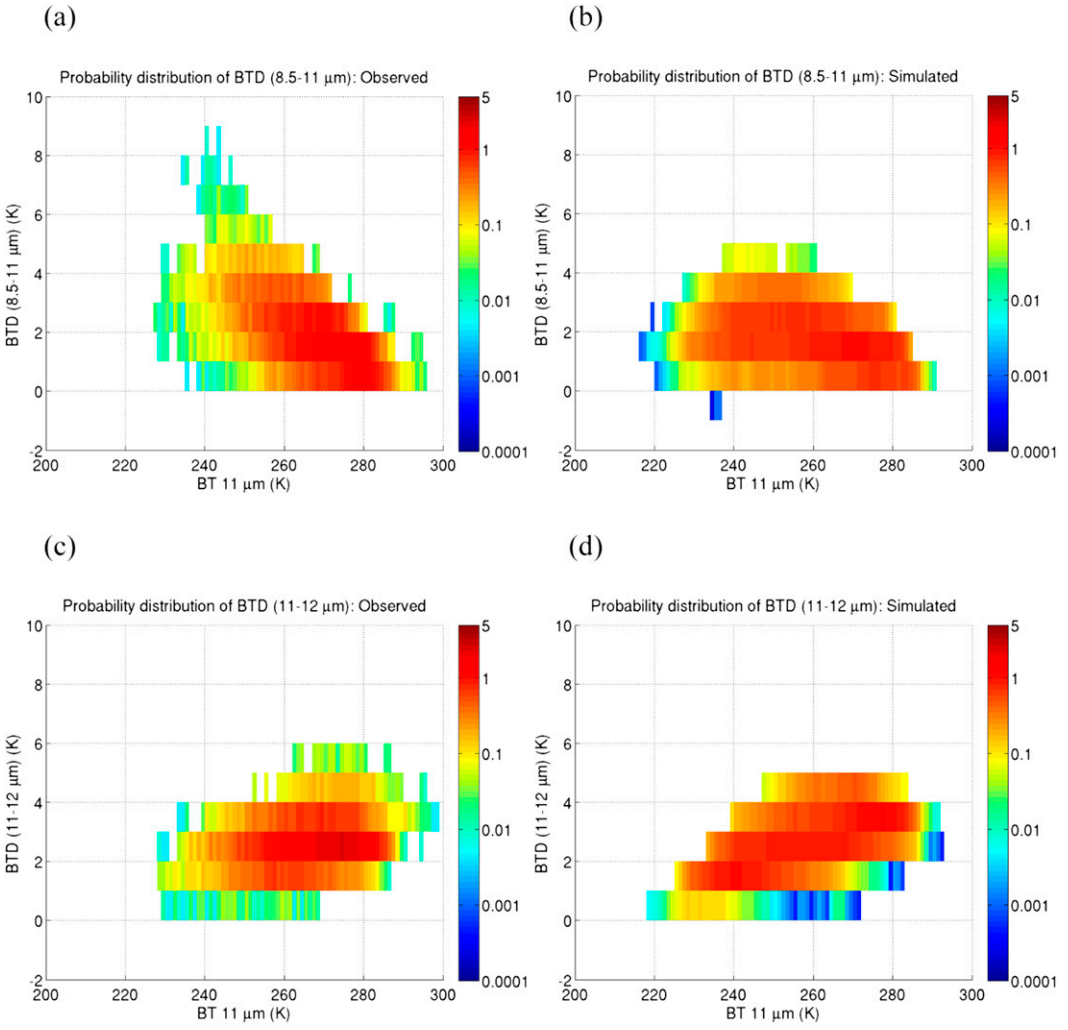

FIG. 5. Probability (%) distributions of (a) observed and (b) simulated 8.5–11-μm BTDs, and (c) observed and (d) simulated 11–12-μm BTDs computed using all thin cirrus grid points with a visible COT < 5 and a CTP < 440 hPa. The distributions are plotted as a function of the 11-μm BTs using all data from the *Aqua* MODIS overpasses during the WRF simulation on 4 Jun 2005.

In this area, MODIS observations show optically very thick midlevel (600–700 hPa) clouds, whereas the simulation shows broadly scattered midlevel clouds with some low-level clouds. In general, however, these results indicate that the 8.5–11- and 11–12-μm BTDs are realistically represented in the simulated satellite dataset.

d. BT and BTD of thin cirrus cloud

To more closely examine the capability of the WRF and RT models to properly simulate thin cirrus clouds, Fig. 5 shows 8.5–11- and 11–12-μm BTD probability distributions as a function of 11-μm BT for pixels with CTP < 440 hPa and COT < 5 for *Aqua* overpasses. The 8.5–11- and 11–12-μm BTD probability distributions for *Terra* overpasses are very similar to those for *Aqua* (not shown). The correlation coefficients of 8.5–11- and 11–12-μm BTD probability distributions between the observations and the simulation are 0.81 (0.75) and 0.61 (0.50), respectively, for thin cirrus clouds over *Aqua* (*Terra*) swaths. The correlation coefficients for 8.5–11-μm (11–12 μm) BTD are increased (decreased) from those of the all-sky conditions (Table 1). Overall, the simulated and observed datasets contain a similar percentage of grid points with positive 8.5–11- and 11–12-μm BTDs; however, the lack of BTDs larger than 5 K indicates that some clouds are not well represented in the simulation. These portions represent a very small fraction of all grid points; thus, the similar range in BTD values indicates that most ice clouds and their associated ice-scattering properties are realistically represented by the microphysics scheme and by the RT model. Of greater concern,

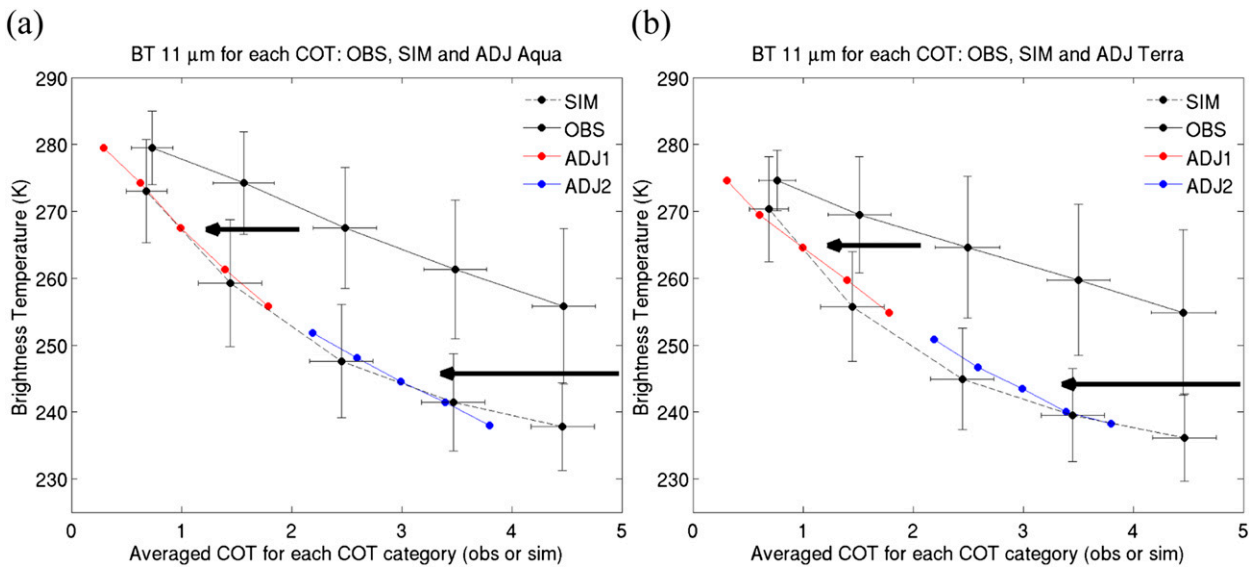

FIG. 6. Averaged BT at MODIS 11-μm vs averaged visible COT for each visible COT category range (0–1, 1–2, 2–3, 3–4, and 4–5 from the left) for the observed (solid fill) and the simulated (dashed fill) thin cirrus clouds from all of the MODIS overpasses of (a) *Aqua* and (b) *Terra* on 4 Jun 2005. Vertical and horizontal error bars indicate the standard deviations of BT and COT, respectively. The simple adjustment (red and blue fill) for MODIS observation is included. The simple adjustment assumes that the MODIS-observed visible COT is 2.5 times that of the simulation. Red filled circles are for COT categories from 0–1 through 4–5, and blue filled circles are for COT categories from 5–6 through 9–10. The arrows indicate the rescaling of the MODIS-observed visible COT.

however, is the tendency for the optically thin simulated clouds with 8.5–11- and 11–12-μm BTDs less than 4 K to have a larger proportion in colder 11-μm BT bins compared to the observations.

CTP is widely distributed over the 11-μm BT range (not shown) and the correlation coefficients between CTP and 11-μm BT are less than 0.22 for both observed and simulated thin cirrus clouds over the *Aqua* and *Terra* swaths. Thus, there should be another factor that causes the increased number of colder simulated 11-μm BTs. Since the COT of cirrus clouds typically increases as the 11-μm BT decreases (Baum et al. 2000b), the colder simulated 11-μm BT suggests that differences in the simulated and retrieved COT values may contribute to the differences in the cirrus cloud BTs. Figure 6 shows the averaged 11-μm BTs for simulated and observed thin cirrus clouds computed for 1-unit COT increments from 0 to 5. Large BT errors are present at 11 μm, with the observed BT averaging 16.2 and 15.3 K warmer than the simulated BTs with the standard deviations of 5.5 and 6.7 K for *Aqua* and *Terra* swaths, respectively. Similar errors are also present in the 8.5- and 12-μm bands (not shown). Holz et al. (2011) found that the asymmetry factors in the visible and near-infrared MODIS bands used to retrieve COT are overestimated by ~30%–40% in the MODIS collection 5 dataset. This error causes the MODIS COT retrievals to be overestimated by around a factor of 2 for thin cirrus clouds when compared with other sensors such as the *Cloud–Aerosol Lidar and Infrared Pathfinder Satellite Observation* (*CALIPSO*; Holz et al. 2009, 2011). Because the MODIS COT is too large for optically thin clouds, this introduces an apparent mismatch in the simulated and observed cirrus cloud samples for COT < 5. Hence, the MODIS-observed cloud sample will be dominated by clouds with a true COT of far less than 5, whereas the simulated cloud distribution will sample the full range from 0 to 5. This bias helps explain the large proportion of simulated clouds with colder 11-μm BTs in Figs. 5b and 5d. Optically thinner clouds are less opaque to upwelling radiation from warmer layers below the clouds and, therefore, appear warmer than optically thicker clouds at the same altitude. Thus, given this bias, it is reasonable to expect that the observed MODIS 11-μm BTs for optically thicker cirrus clouds will be comparable to the simulated BTs for optically thinner cirrus. The shift toward colder BTs in the synthetic datasets supports this expectation. Simply adjusting the observation dataset to 2.5 times smaller COT (red filled circles in Fig. 6) greatly reduces the magnitude of the BT bias between the simulation and observations. This is broadly consistent with the factor of 2 MODIS COT bias discussed in Holz et al. (2009, 2011); however, the small difference in the ratio suggests that the simulated clouds may be optically too thin. The adjustment of the MODIS-observed COT category in Fig. 6 includes larger MODIS-observed COT

values (5–10), indicated as blue filled circles. The much closer correspondence between the observed and simulated BTs for larger MODIS-observed COT attained with this simple adjustment suggests that the overestimation of MODIS-observed COT may be valid for a large range of clouds up to a visible COT value of 10.

To find out the effects of a possible ancillary data bias, several sensitivity tests are performed including the addition and subtraction of 2 K and 10% for WRF temperature water vapor profiles, respectively, to obtain the simulated BT and CTP. The bias ranges are based on previous studies (Lee et al. 2014; Schmit et al. 2008), which showed that the standard deviation and the root-mean-square error of the NWP model temperature and water vapor profiles are around (or below) 2 K and 10%, respectively, in the middle and lower troposphere compared with radiosonde observations. The sensitivity tests show that some differences may come from the errors in ancillary data bias, but the revelation about the overestimation of MODIS COT retrieved for thin cirrus clouds is not affected by the ancillary data bias including the WRF temperature–water vapor profiles (not shown).

Taken together, these results show that the simulated COT and infrared BT results are realistically depicted for most optically thin ice clouds if allowance is made for the high bias in the MODIS COT retrievals.

4. Summary

In this study, simulated BTs computed using cloud, temperature, and water vapor profiles from a high-resolution WRF model simulation over the CONUS on 4 June 2005 were compared with real MODIS satellite observations, with an emphasis on evaluating the accuracy of optically thin cirrus clouds. Overall, the location and magnitude of the simulated 11-μm MODIS BTs were consistent with the observations when all cloud types are considered. Compared with observations, the simulated ice and water cloud features are reasonably depicted in the 8.5–11- and 11–12-μm BTD fields. The correlation coefficients between the observed and simulated 8.5–11- and 11–12-μm BTD probability distributions for thin cirrus clouds are 0.81 (0.75) and 0.61 (0.50), respectively, for *Aqua* (*Terra*) swaths. Although the range of positive BTD values is similar in the observed and simulated distributions for MODIS pixels with visible COT less than 5, the corresponding simulated 11-μm BTs are generally much colder than the observations. The mean difference between the simulated and observed 11-μm BTs (averaged for 1-unit COT increments) is over 15 K in magnitude and the standard deviation is over 5.5 K for both *Aqua* and *Terra* swaths. Because the MODIS COT is too large for optically thin cirrus clouds, the positive COT bias contributes to the generally warmer observed MODIS BT by erroneously excluding clouds with slightly higher COTs and colder infrared BTs from the observed cloud samples. After accounting for this discrepancy, the apparent cold BT bias in the synthetic dataset for optically thin cirrus clouds was greatly reduced. Taken together, these results indicate that the combined WRF and RT modeling framework is able to realistically simulate cloud properties, including those for optically thin cirrus clouds.

Acknowledgments. This work was funded under the National Oceanic and Atmospheric Administration under Cooperative Agreement NA06NES4400002. Additional support was provided by the TeraGrid supercomputing network under Grant ATM060029 and by the National Center for Supercomputing Applications (NCSA) at the University of Illinois. Special thanks are given to Gerardo Cisneros and to the NCSA personnel for their help with the WRF simulation, which was performed on the ''cobalt'' supercomputer.

REFERENCES

Ackerman, S. A., W. L. Smith, J. D. Spinhirne, and H. E. Revercomb, 1990: The 27–28 October 1986 FIRE IFO cirrus case study: Spectral properties of cirrus clouds in the 8–12-μm window. *Mon. Wea. Rev.,* **118,** 2377–2388.

Baum, B. A., D. P. Kratz, P. Yang, S. Ou, Y. Hu, P. F. Soulen, and S.-C. Tsay, 2000a: Remote sensing of cloud properties using MODIS Airborne Simulator imagery during SUCCESS. I. Data and models. *J. Geophys. Res.,* **105,** 11 767–11 780.

——, P. F. Soulen, K. I. Strabala, M. D. King, S. A. Ackerman, W. P. Menzel, and P. Yang, 2000b: Remote sensing of cloud properties using MODIS Airborne Simulator imagery during SUCCESS. 2. Cloud thermodynamic phase. *J. Geophys. Res.,* **105,** 11 781–11 792.

——, P. Yang, A. J. Heymsfield, S. Platnick, M. D. King, Y.-X. Hu, and S. T. Bedka, 2005: Bulk scattering properties for the remote sensing of ice clouds. Part II: Narrowband models. *J. Appl. Meteor.,* **44,** 1896–1911.

Bikos, D., and Coauthors, 2012: Synthetic satellite imagery for real-time high-resolution model evaluation. *Wea. Forecasting,* **27,** 784–795.

Chaboureau, J.-P., and J.-P. Pinty, 2006: Evaluation of a cirrus parameterization with Meteosat Second Generation observations. *Geophys. Res. Lett.,* **33,** L03815, doi:10.1029/2005GL024725.

Chen, T., W. B. Rossow, and Y. Zhang, 2000: Radiative effects of cloud-type variations. *J. Climate,* **13,** 264–286.

Chen, Y., Y. Han, and F. Weng, 2012: Comparison of two transmittance algorithms in the Community Radiative Transfer Model: Application to AVHRR. *J. Geophys. Res.,* **117,** D06206, doi:10.1029/2011JD016656.

Daniels, J., W. Bresky, S. Wanzong, C. Velden, and H. Berger, 2012: GOES-R Advanced Baseline Imager (ABI) algorithm theoretical basis document for derived motion winds. NOAA/NESDIS/Center for Satellite Applications and Research,

98 pp. [Available online at http://www.star.nesdis.noaa.gov/goesr/docs/ATBD/DMW.pdf.]

Dessler, A. E., and P. Yang, 2003: The distribution of tropical thin cirrus clouds inferred from *Terra* MODIS data. *J. Climate,* **16,** 1241–1247.

Dudhia, J., 1989: Numerical study of convection observed during the Winter Monsoon Experiment using a mesoscale two-dimensional model. *J. Atmos. Sci.,* **46,** 3077–3107.

Garand, L., and S. Nadon, 1998: High-resolution satellite analysis and model evaluation of clouds and radiation over the Mackenzie basin using AVHRR data. *J. Climate,* **11,** 1976–1996.

Gehlot, S., and J. Quaas, 2012: Convection–climate feedbacks in the ECHAM5 general circulation model: Evaluation of cirrus cloud life cycles with ISCCP satellite data from a Lagrangian trajectory perspective. *J. Climate,* **25,** 5241–5259.

Greenwald, T. J., A. Huang, J. Sieglaff, and E. Olson, 2008: User's manual to the Fast solar/infrared radiative transfer model. Cooperative Institute for Meteorological Satellite Studies, University of Wisconsin—Madison, 23 pp. [Available online at http://cimss.ssec.wisc.edu/goes_r/awg/proxy/forward_model/SOLAR-IR_RT_MODEL_Users_Manual.pdf.]

——, Y.-K. Lee, J. A. Otkin, and T. L'Ecuyer, 2010: Evaluation of midlatitude clouds in a large-scale high-resolution simulation using CloudSat observation. *J. Geophys. Res.,* **115,** D19203, doi:10.1029/2009JD013552.

Han, M., S. A. Braun, T. Matsui, and C. R. Williams, 2013: Evaluation of cloud microphysics schemes in simulations of a winter storm using radar and radiometer measurements. *J. Geophys. Res.,* **118,** 1401–1419, doi:10.1002/jgrd.50115.

Han, Q., W. Rossow, R. Welch, A. White, and J. Chou, 1995: Validation of satellite retrievals of cloud microphysics and liquid water path using observations from FIRE. *J. Atmos. Sci.,* **52,** 4183–4195.

Heidinger, A. K., C. O'Dell, R. Bennartz, and T. Greenwald, 2006: The successive-order-of-interaction radiative transfer model. Part I: Model development. *J. Appl. Meteor. Climatol.,* **45,** 1388–1402.

Heymsfield, A. J., S. Matrosov, and B. Baum, 2003: Ice water path–optical depth relationships for cirrus and deep stratiform ice cloud layers. *J. Appl. Meteor.,* **42,** 1369–1390.

Holz, R., A. Heidinger, D. Turner, S. Ackerman, R. Kuehn, M. Vaughn, and S. Platnick, 2009: Uncertainties of cirrus OD retrievals from active and passive A-Train measurements. *CloudSat/CALIPSO Science Workshop,* Madison, WI, CIMMS/University of Wisconsin-Madison.

——, and Coauthors, 2011: Finding closure between V3 CALIOP and MODIS optical depth retrievals using IR observations. Abstracts, *2011 Fall Meeting,* San Francisco, CA, Amer. Geophys. Union, Abstract A23F-03. [Available online at http://abstractsearch.agu.org/meetings/2011/FM/sections/A/sessions/A23F/abstracts/A23F-03.html.]

Jankov, I., and Coauthors, 2010: An evaluation of five ARW-WRF microphysics schemes using synthetic GOES imagery for an atmospheric river event affecting the California coast. *J. Hydrometeor.,* **12,** 618–633.

Keil, C., A. Tafferner, H. Mannstein, and U. Schattler, 2003: Evaluating high-resolution model forecasts of European winter storms by use of satellite and radar observations. *Wea. Forecasting,* **18,** 732–747.

Lee, Y.-K., P. Yang, Y. Hu, B. A. Baum, N. G. Loeb, and B.-C. Gao, 2006: Potential nighttime contamination of CERES clear-sky fields of view by optically thin cirrus during the CRYSTAL-FACE campaign. *J. Geophys. Res.,* **111,** D09203, doi:10.1029/2005JD006372.

——, T. Greenwald, P. Yang, S. Ackerman, and H.-L. Huang, 2010: Global distribution of instantaneous daytime radiative effects of high thin clouds observed by the cloud profiling radar. *J. Appl. Remote Sens.,* **4,** 043543, doi:10.1117/1.3491858.

——, Z. Li, J. Li, and T. J. Schmit, 2014: Evaluation of the GOES-R ABI LAP retrieval algorithm using the *GOES-13* Sounder. *J. Atmos. Oceanic Technol.,* **31,** 3–19.

Li, J., and Coauthors, 2012: GOES-R Advanced Baseline Imager (ABI) algorithm theoretical basis document for legacy atmospheric moisture profile, legacy atmospheric temperature profile, total precipitable water, and derived atmospheric stability indices. NOAA/NESDIS/Center for Satellite Applications and Research, 108 pp. [Available online at http://www.star.nesdis.noaa.gov/goesr/docs/ATBD/LAP.pdf.]

Lopez, P., K. Finkele, P. Clark, and P. Mascart, 2003: Validation and intercomparison of three FASTEX cloud systems: Comparison with coarse-resolution simulations. *Quart. J. Roy. Meteor. Soc.,* **129,** 1841–1871.

McMillin, L. M., X. Xiong, Y. Han, T. J. Kleespies, and P. Van Delst, 2006: Atmospheric transmittance of an absorbing gas. 7. Further improvements to the OPTRAN 6 approach. *Appl. Opt.,* **45,** 2028–2034, doi:10.1364/AO.45.002028.

Mellor, G. L., and T. Yamada, 1982: Development of a turbulence closure model for geophysical fluid problems. *Rev. Geophys. Space Phys.,* **20,** 851–875.

Menzel, W. P., W. L. Smith, and T. R. Stewart, 1983: Improved cloud motion wind vector and altitude assignment using VAS. *J. Appl. Meteor.,* **22,** 377–384.

——, R. A. Frey, and B. A. Baum, 2010: Cloud top properties and cloud phase algorithm theoretical basis document. NASA GSFC, 62 pp. [Available online at http://modis.gsfc.nasa.gov/data/atbd/atbd_mod04.pdf.]

Mlawer, E. J., S. J. Taubman, P. D. Brown, and M. J. Iacono, 1997: Radiative transfer for inhomogeneous atmospheres: RRTM, a validated correlated-*k* model for the longwave. *J. Geophys. Res.,* **102,** 16 663–16 682.

Morcrette, J.-J., 1991: Evaluation of model-generated cloudiness: Satellite-observed and model-generated diurnal variability of brightness temperature. *Mon. Wea. Rev.,* **119,** 1205–1224.

Nam, C. C. W., and J. Quaas, 2012: Evaluation of clouds and precipitation in the ECHAM5 general circulation model using *CALIPSO* and *CloudSat* satellite data. *J. Climate,* **25,** 4975–4992.

Otkin, J. A., and T. J. Greenwald, 2008: Comparison of WRF model-simulated and MODIS-derived cloud data. *Mon. Wea. Rev.,* **136,** 1957–1970.

——, H.-L. Huang, T. Greenwald, E. R. Olson, and J. Sieglaff, 2007a: Large-scale WRF-simulated proxy atmospheric profile datasets used to support GOES-R research activities. *Proc. 15th Conf. on Satellite Meteorology and Oceanography,* Amsterdam, Netherlands, EUMETSAT–Amer. Meteor. Soc., 5 pp. [Available online at http://www.eumetsat.int/website/wcm/idc/idcplg?IdcService=GET_FILE&dDocName=PDF_CONF_P50_S9_01_OTKIN_P&RevisionSelectionMethod=LatestReleased&Rendition=Web.]

——, D. J. Posselt, E. R. Olson, H.-L. Huang, J. E. Davies, J. Li, and C. S. Velden, 2007b: Mesoscale numerical weather prediction models used in support of infrared hyperspectral measurements simulation and product algorithm development. *J. Atmos. Oceanic Technol.,* **24,** 585–601.

——, T. J. Greenwald, J. Sieglaff, and H.-L. Huang, 2009: Validation of a large-scale simulated brightness temperature dataset using SEVIRI satellite observations. *J. Appl. Meteor. Climatol.,* **48,** 1613–1626.

Platnick, S., M. D. King, S. A. Ackerman, W. P. Menzel, and B. A. Baum, 2003: The MODIS cloud products: Algorithms and examples from *Terra*. *IEEE Trans. Geosci. Remote Sens.,* **41,** 459–473.

Platt, C. M. R., and Harshvardhan, 1988: Temperature dependence of cirrus extinction: Implications for climate feedback. *J. Geophys. Res.,* **93,** 11 051–11 058.

Ringer, M. A., J. M. Edwards, and A. Slingo, 2003: Simulation of satellite channel radiances in the Met Office Unified Model. *Quart. J. Roy. Meteor. Soc.,* **129,** 1169–1190.

Satoh, M., T. Inoue, and H. Miura, 2010: Evaluation of cloud properties of global and local cloud system resolving models using *CALIPSO* and *CloudSat* simulators. *J. Geophys. Res.,* **115,** D00H14, doi:10.1029/2009JD012247.

Schmit, T. J., M. M. Gunshor, W. P. Menzel, J. Li, S. Bachmeier, and J. J. Gurka, 2005: Introducing the next-generation Advanced Baseline Imager (ABI) on GOES-R. *Bull. Amer. Meteor. Soc.,* **86,** 1079–1096.

——, J. Li, J. Li, W. F. Feltz, J. J. Gurka, M. D. Goldberg, and K. J. Schrab, 2008: The GOES-R Advanced Baseline Imager and the continuation of current sounder products. *J. Appl. Meteor. Climatol.,* **47,** 2696–2711.

——, and Coauthors, 2012: GOES-R Advanced Baseline Imager (ABI) algorithm theoretical basis document for cloud and moisture imagery product (CMIP). NOAA/NESDIS/Center for Satellite Applications and Research, 63 pp. [Available online at http://www.star.nesdis.noaa.gov/goesr/docs/ATBD/Imagery.pdf.]

Seemann, S. W., E. E. Borbas, R. O. Knuteson, G. R. Stephenson, and H.-L. Huang, 2008: Development of a global infrared land surface emissivity database for application to clear sky sounding retrievals from multispectral satellite radiance measurements. *J. Appl. Meteor. Climatol.,* **47,** 108–123.

Skamarock, W. C., J. B. Klemp, J. Dudhia, D. O. Gill, D. M. Barker, W. Wang, and J. G. Powers, 2005: A description of the Advanced Research WRF version 2. NCAR Tech. Note NCAR/TN–468+STR, 88 pp.

Strabala, K. I., S. A. Ackerman, and W. P. Menzel, 1994: Cloud properties inferred from 8–12-μm data. *J. Appl. Meteor.,* **33,** 212–229.

Sun, Z., and L. Rikus, 2004: Validating model clouds and their optical properties using geostationary satellite imagery. *Mon. Wea. Rev.,* **132,** 2006–2020.

Thompson, G., P. R. Field, R. M. Rasmussen, and W. D. Hall, 2008: Explicit forecasts of winter precipitation using an improved bulk microphysics scheme. Part II: Implementation of a new snow parameterization. *Mon. Wea. Rev.,* **136,** 5095–5115.

Tselioudis, G., and C. Jakob, 2002: Evaluation of midlatitude cloud properties in a weather and a climate model: Dependence on dynamic regime and spatial resolution. *J. Geophys. Res.,* **107,** 4781, doi:10.1029/2002JD002259.

Wylie, D. P., and W. P. Menzel, 1999: Eight years of high cloud statistics using HIRS. *J. Climate,* **12,** 170–184.

Yu, W., M. Doutriaux, G. Seze, H. Le Treut, and M. Desbois, 1996: A methodology study of the validation of clouds in GCMs using ISCCP satellite observation. *Climate Dyn.,* **12,** 389–401.

Zhang, Y., B. Rockel, R. Stuhlmann, R. Hollmann, and U. Karstens, 2001: REMO cloud modeling: Improvements and validation with ISCCP DX data. *J. Appl. Meteor.,* **40,** 389–408.